Separation and Purification Technology 359 (2025) 130477

Contents lists available at ScienceDirect

Separation and Purification Technology

journal homepage: www.elsevier.com/locate/seppur

Four-bed vacuum pressure swing adsorption for xenon recycling from semiconductor waste gas

YeonJi Choi [a], Kyung Min Choi [a,b,*], Kyungtae Park [a,b,*]

[a] Department of Chemical and Biological Engineering, Sookmyung Women's University, Seoul 04310, Republic of Korea
[b] Institute of Advanced Materials and Systems, Sookmyung Women's University, Seoul 04310, Republic of Korea

ARTICLE INFO

Handling editor: Z Bao

Keywords:
Xenon separation
Vacuum pressure swing adsorption
Process simulation
Economic analysis
Global warming potential analysis

ABSTRACT

The development of the space industry, increasing semiconductor production, and growing demand for medical xenon has significantly boosted the xenon market. However, the commercial production of cryogenic distillation is an energy intensive process and results in economic and environmental issues. In this study, experimental adsorbent data collection and a vacuum pressure swing adsorption (VPSA) simulation are presented for recovering and purifying xenon from semiconductor waste gas containing 0.1 mol% Xe and 99.9 mol% N_2. FMOFCu was used for xenon adsorption, and the adsorption data were collected through isotherm and breakthrough experiments using Xe and N_2. Further, the VPSA process was designed and parametric studies were conducted using gPROMS simulations based on experimental data. Consequently, 99.9 % of the xenon product was produced through a two-stage VPSA process, and an economic and environmental evaluation of the produced xenon was conducted. The minimum selling price of the produced xenon ranged from 554.42 to 1482.08 $/kgXe, which was more than 1000 $/kgXe lower than the current wholesale price of xenon. The electricity consumption of the proposed VPSA process was 40.99 kWh, and the calculated global warming potential was 28.92 kg CO_2 eq for 1 kg of Xe produced. Therefore, the proposed VPSA process was economical and environmentally sustainable.

1. Introduction

Xenon is an extremely rare inert gas that comprises only 0.000009 mol% of the atmosphere [1]. It is widely used in the aerospace, medicine, lighting, and semiconductor manufacturing industries [2–4]. Recent technological advancements have led to a significant increase in the demand for using xenon in laser processes within the semiconductor industry [5]. Consequently, the global market for xenon production reached USD 523.62 million in 2023 [6]. This increased industrial demand for xenon in recent years has led to extensive research on xenon production [4,7–9].

Xenon is primarily produced as a by-product of air separation units (ASUs) through an additional highly energy-intensive process [10]. The ASUs operate at cryogenic temperatures and demand a substantial amount of electricity [11], which results in significant carbon emissions. The primary purpose of ASUs is to produce oxygen and nitrogen, and therefore, xenon production is constrained by the quantitative and geographic demand for these gases [12]. The insufficient supply and transportation costs of xenon have driven up its price. Further, various economic factors such as the Russia–Ukraine War and China's environmental regulations have hindered active production and trade, causing and increase and fluctuations in xenon prices [13]. Consequently, the wholesale price for xenon has remained very high and unstable in recent years, increasing from $15/L in 2020 to $100/L in 2022, before dropping to $60/L by 2023 [14].

Therefore, current research is focusing on developing new production methods for xenon using various processes such as membrane separation, gas hydration, and adsorption as alternatives to the traditional methods. [15] attempted to separate xenon using a hybrid process that combined gas hydrates and cryogenic distillation. High-purity xenon can be produced by concentrating the ASU byproducts through has hydrates and then using cryogenic distillation, while reducing electricity consumption. [16] investigated xenon separation from natural gas by combining gas hydrate crystallization with a membrane process. They used natural gas as the feed to separate xenon, methane, and carbon dioxide and achieved a high recovery rate by hydrating xenon. Petukhov et al. [17] separated xenon from natural gas by integrating batch distillation with a membrane process. They used the obtained high-purity xenon feed at the primary concentration to achieve ultra high-purity xenon production. Miandoab et al. [18] produced xenon through membrane separation using feed gas derived from the

* Corresponding authors.
E-mail address: ktpark@sm.ac.kr (K. Park).

https://doi.org/10.1016/j.seppur.2024.130477
Received 18 September 2024; Received in revised form 29 October 2024; Accepted 9 November 2024
Available online 14 November 2024

Nomenclature

Symbols

$b_{0,i}$	Affinity constant of the Langmuir model
C_i	Concentration of component i in the bulk fluid phase
$C_{p,solid}$	Heat capacity of the adsorbent material
$C_{p,w}$	Specific heat capacity of the wall material
D	Dispersion coefficient
d_{bed}	Diameter of the adsorption bed
d_{pellet}	Pellet particle diameter
$F_{N_2,i}$	Molar flowrate of nitrogen in stream i
$F_{Xe,i}$	Molar flowrate of xenon in stream i
$\widetilde{H}_{ads,i}$	Molar specific enthalpy of component i in adsorbed phase
H_f	Bulk fluid phase mass specific enthalpy
ΔH_i	Isosteric adsorption heat
h_{f-w}	Heat transfer coefficient between the bulk fluid and wall
h_{w-a}	Heat transfer coefficient from the bed wall to the ambient environment
k_i	Lumped linear driving force mass transfer coefficient for component i
l_w	Bed wall thickness
$N_{ads-mass,i}$	Rate of mass transfer for component i from the fluid to the adsorbed phase
n_{cycle}	Number of cycles per year
P	Pressure of the bulk fluid
P_i	Partial pressure of component i.
q_i	Saturated adsorption capacity of component i
$\overline{q_i}$	Average adsorbed amount
$\overline{q_i^*}$	Average equilibrium amount adsorbed, in equilibrium
R_g	Gas constant
Sc	Schmidt number
T_a	Ambient temperature
T_f	Temperature of the bulk fluid
$T_{ref,solid}$	Reference temperature of the energy of the adsorbent material
T_s	Solid phase temperature
T_w	Temperature of the wall
t	Time
t_{cycle}	Total time of a cycle
$\widehat{U}_{bed}$	Energy per unit volume of the bed
v_{sup}	Fluid phase superficial velocity
w_i	Mass fraction of component i in fluid phase
z	Distance along the axial direction

Abbreviations

AD	Adsorption step
ASU	Air separation unit
BD	Blowdown step
EC	Environment cost
ED	Pressure equalization (depressurization) step
ER	Pressure equalization (re-pressurization) step
ETS	Emission trading system
GWP	Global warming potential
ID	Idle step
MSP	Minimum selling price
MTC	Mass transfer coefficient
PR	Re-pressurization step
PU	Puring step
TCC	Total capital cost
TEC	Total equipment cost
TOC	Total operating cost
VPSA	Vacuum pressure swing adsorption

Greek symbols

ε	Both inter- and intra- particle voids
ε_{bed}	Inter-particle voids
λ_{eff}	Effective thermal conductivity
λ_w	Thermal conductivity of the wall material
μ	Dynamic viscosity
ρ_{bed}	Bed bulk density
ρ_T	Total mass density of the fluid phase
ρ_w	Mass density of the wall material

ASU. Their membrane process separated xenon and krypton in a single step. Hansen et al. [4] performed a cost-benefit analysis of capturing xenon during the aqueous solution reprocessing of spent nuclear fuel. They found that this process was not essential and the cost of capturing xenon ranged from $71.50/L to $131.13/L, which was higher than the market price of xenon. Yoshida et al. [19] demonstrated a two-stage, four-bed PSA system using zeolite, MS-13X to concentrate xenon in atmospheric air (0.1 ppm) to 400 ppm, demonstrating the feasibility of the PSA process for xenon enrichment. They also developed Enriching Reflux PSA (ER-PSA) Process with parallel equalization using same adsorbent, achieving an 80-fold concentration of xenon from 18 ppm [20]. Willion et al. [21] developed a PSA unit using activated charcoal for xenon capture and enrichment for the detection of radioactive xenon isotopes in the atmosphere, achieving a 1000-fold increase in the concentration of airborne xenon. Schell et al. [22] also developed an integrated PSA unit and measurement system using molecular sieve carbon, achieving a 107-fold xenon purification for the detection of radioactive xenon released into the atmosphere. Yamawaki et al. [23] developed a process to recycle waste gas from a plasma process. They achieved a xenon gas purity of 99.98 % and a recovery rate of 99.999 % by using a PSA process with activated carbon to separate xenon and various other components. However, the feed gas used in their experiments contained a significantly higher xenon concentration (28.5–50 %) compared to actual waste gases.

Previous studies showed that the xenon separation process requires a significant amount of energy. However, to the best of our knowledge, the environmental and economic effects of the high energy consumption in this process have rarely been evaluated. Analyzing the economic and environmental impacts of the xenon separation process are crucial for developing a sustainable xenon production process.

Furthermore, the studies mentioned above using PSA systems for xenon enrichment did not achieve high-purity xenon when they used ppm levels of atmospheric xenon. Therefore, research is needed on feed gases that contain higher xenon concentrations than air, which may include exhaust gases from processes utilizing xenon. This research provides a foundation for producing high-purity xenon using feed gases with a composition like that of discarded semiconductor waste gases.

The xenon concentration in semiconductor waste gas is approximately 10,000 times higher than that in air [24]. Xenon production was studied to recycle semiconductor waste gas through a pressure swing adsorption (PSA) process using metal–organic frameworks (MOFs). The MOF has attracted attention as an adsorbent for xenon separation because it can produce thousands of different pores based on the fabrication methods, making MOFs well-suited for developing adsorbents required for applications. [25] demonstrated the potential of MOFs for xenon separation.

PSA is a widely commercialized mild process that has low electricity consumption [26]. Therefore, in this study, the electricity consumption for the xenon separation process through PSA using MOFs is calculated and an economic evaluation is performed using facilities and operating

funds. In addition, the sustainability of the developed process was verified through environmental evaluation. To this end, a four-bed vacuum pressure swing adsorption (VPSA) process using MOFs was developed and evaluated for xenon recycling. The configuration and cycle schedule of the proposed VPSA process were designed, and experiments were conducted to measure the adsorption isotherms and breakthrough characteristics of Xe and N_2 on FMOFCu. A gPROMS simulation was performed using the experimental data to determine the operational conditions, production rates, and electricity consumption of the xenon production process. Parametric studies of the process conditions were also performed. Further, the data from the simulation were compared with the wholesale xenon prices obtained through economic analysis, and an environmental assessment based on electricity consumption was conducted to evaluate the sustainability of the xenon production process compared to that of traditional method.

The remainder of this paper is organized as follows. Section 2 outlines the proposed VPSA process and simulation configuration. Section 3 outlines and discusses the results. Finally, the conclusions are presented in Section 4.

2. Methodology

2.1. Process description

A two-stage, four-bed VPSA process was designed for producing a product gas with a Xe concentration of 99.9 % from the semiconductor production exhaust gas (N_2 = 99.9 %, Xe = 0.1 %) [24] for recycling. The schematic diagram of the four-bed VPSA process is depicted in Fig. 1.

The feed gas is supplied to Bed 1 in the adsorption step, wherein xenon is adsorbed on the adsorbent and nitrogen-enriched waste gas is released into the waste gas stream. Bed 2 was repressurized to prepare for the adsorption step. The waste gas from Bed 1 is partially transferred to Bed 2 for pressurization. Bed 3 in the desorption (purging) step receives a portion of the waste gas from Bed 1 as a purging gas to facilitate the desorption of Xe, resulting in a Xe-enriched product stream. Bed 4 in the depressurization (blowdown) step is used to prepare for the desorption step. According to the cycle schedule, each bed goes through all steps.

Unlike other PSA purification processes that contain more than 10 % of the product in the feed stream [27–31], the process in this study contained only trace amounts of the product (0.1 %). Therefore, the basic structure of PSA was modified in two stages to achieve the target purity (99.9 %). First, the gas generated during blowdown was separated from the product because xenon did not desorb properly unless it was under a sufficiently low pressure [24]. However, the separation led to recovery losses caused by desorption during blowdown. Therefore, to minimize xenon loss, the blowdown was performed in a co-current direction with the feed. When the feed flowed in the same direction as the blowdown, pressure drops during the blowdown step occurred on the opposite site of the column, where the adsorption was intense in the feed step. This helps prevent direct desorption during the blowdown step and reduces the xenon loss.

2.2. Cycle schedule for the four-bed VPSA

The Skarstrom cycle [32], which consists of adsorption, depressurization (blowdown), desorption (purging), and re-pressurization, was the first PSA cycle to be developed. This PSA cycle continues to be widely utilized, and various advanced PSA processes have been developed and commercialized based on this cycle[30,33–36]. In this study, a modified Skarstrom cycle was used to reduce the unnecessary energy consumption by adding two pressure equalization steps to compensate for the large amount of energy required by the VPSA cycle structure of swinging under high pressure and vacuum[33,37]. A detailed cycle schedule, graphical overview, and detailed steps are presented in Fig. 2. In addition, a detailed description of each step is provided in Appendix B.

2.3. Simulation details

A commercial process simulator gPROMS (Version 2022.1.0), which is a rigorous modeling tool for dynamic processes, was used to design the process for each stage. All governing equations used in the developed model are summarized in Table A1 in Appendix A.

The assumptions for the modeling are summarized as follows:

- VPSA process is operated under the non-isotherms condition.

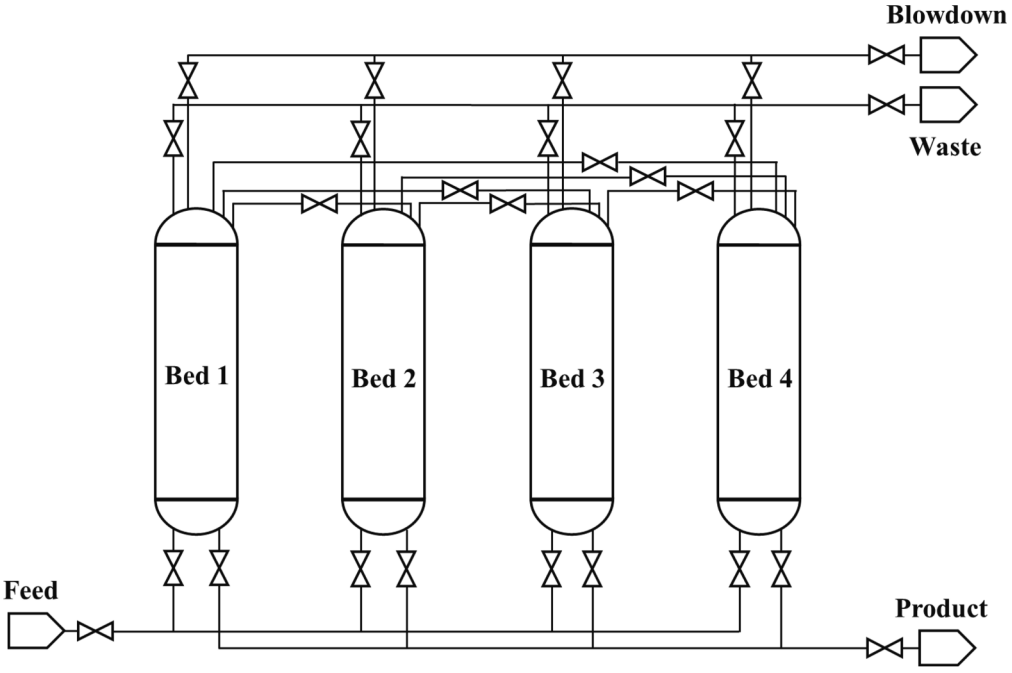

Fig. 1. Schematic of the modified four-bed VPSA system.

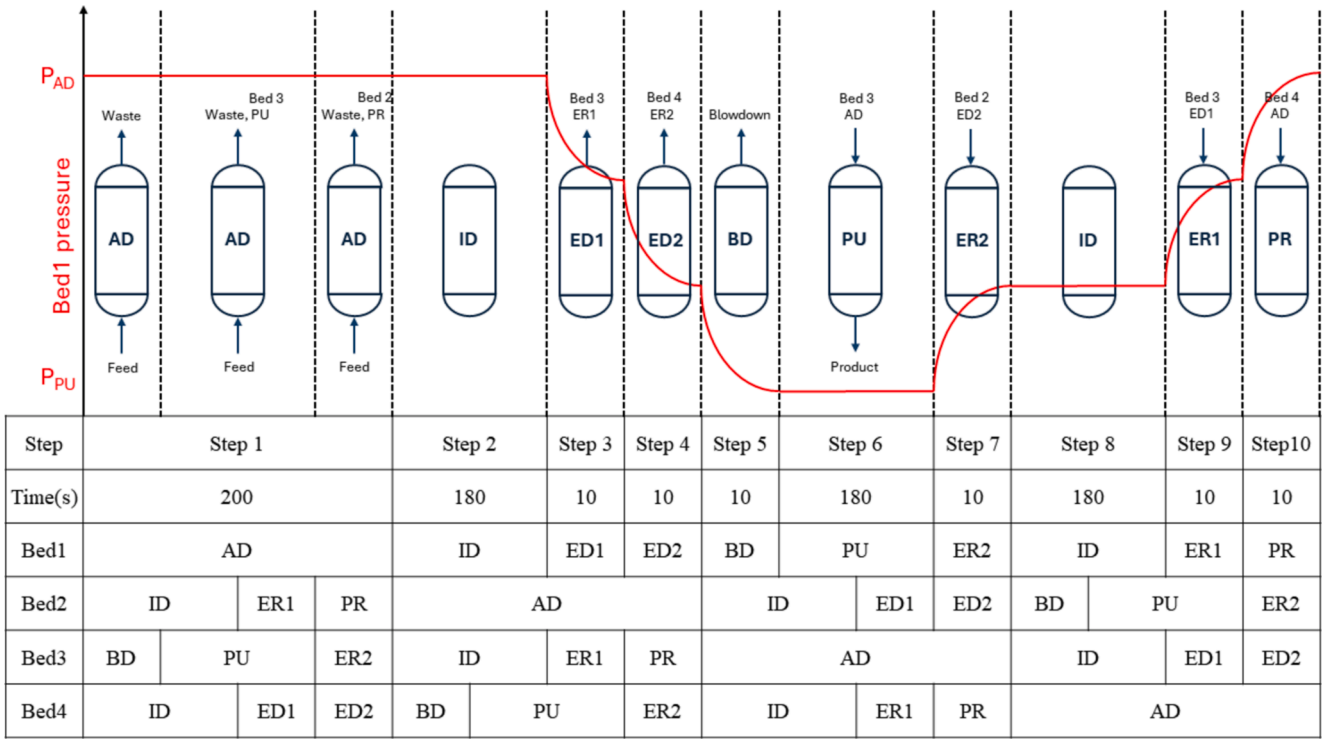

Step	Step 1	Step 2	Step 3	Step 4	Step 5	Step 6	Step 7	Step 8	Step 9	Step10
Time(s)	200	180	10	10	10	180	10	180	10	10
Bed1	AD	ID	ED1	ED2	BD	PU	ER2	ID	ER1	PR
Bed2	ID	ER1	PR	AD		ID	ED1	ED2	BD	PU	ER2
Bed3	BD	PU	ER2	ID	ER1	PR	AD		ID	ED1	ED2
Bed4	ID	ED1	ED2	BD	PU	ER2	ID	ER1	PR	AD

Fig. 2. Details of the cycle schedule of the modified four-bed VPSA process. In this figure, AD, ID, ED, BD, PU, ER, and PR represent adsorption, idle, pressure equalization (depressurization), blowdown, desorption (purging), pressure equalization (re-pressurization), and repressurization, respectively.

- Peng–Robinson equation is used as a thermodynamic model.
- Flow in a radial direction is ignored.
- Number of discretization points per bed layer is set to 30.
- Initial composition of the adsorption bed is 100 % N_2.
- Target xenon purity of the final product is 99.9 %.
- The feed gas is supplied after passing through the water guard bed. The humidity requirement is 5 ppm or less.

2.3.1. Bed properties

Table 1 summarizes the input parameters for the base case and the specifications of the adsorption bed. The flow rate, adsorption pressure, desorption pressure, and bed size were set based on experience-based knowledge. The bed porosity and bulk density were obtained based on in-house experimental results.

The performance of the process was evaluated based on the purity and recovery of the product. The purity, recovery, and productivity equations are defined in Eqns. (1)–(3).

$$Xepurity[\%] = \frac{\int_0^{t_{cycle}} F_{Xe,i}dt}{\int_0^{t_{cycle}} (F_{Xe,i} + F_{N_2,i})dt} \times 100 \quad (1)$$

$$Xerecovery[\%] = \frac{\int_0^{t_{cycle}} F_{Xe,i}dt}{\int_0^{t_{cycle}} F_{Xe,feed}dt} \times 100 \quad (2)$$

$$Xeannualproductivity[kmol/yr] = n_{cycle} \times \int_0^{t_{cycle}} F_{Xe,i}dt \quad (3)$$

where, t_{cycle}, $F_{Xe,i}$, $F_{N_2,i}$, and n_{cycle} represent the total time of a cycle, molar flowrate of xenon in stream I, molar flowrate of nitrogen in stream i (i ∈ {feed, product, waste, blowdown}), and number of cycles per year, respectively.

PSA is inherently a dynamic process, wherein all variables in a system change over time until they reach a cyclic steady state. In this study, the cyclic steady state was assumed to be reached when the change in both product purity and recovery between cycles was less than 10^{-4}.

2.3.2. Adsorbent properties

FMOFCu was employed as an adsorbent for xenon separation in the proposed VPSA process. In-house experiments were conducted to obtain the data for the adsorbent. In addition, the adsorption properties were characterized via adsorption equilibrium isotherm measurements of each component and breakthrough tests. The physical properties of the bed obtained from these measurements are summarized in Table 2.

The adsorption equilibrium isotherm test at 298 K showed that the

Table 1
Input parameters of base case of the first-stage VPSA and specification of the bed.

Condition	Value	Bed data	Value
Feed flowrate [kmol/h]	10	Adsorption bed length [m]	1.4
Adsorption pressure [bar]	8	Bed inner diameter [m]	0.14
Desorption pressure [bar]	0.002	Bed porosity	0.474*
Feed temperature [K]	303	Bed bulk density [kg/m^3]	630*
Xenon molar concentration [%]	0.1	Initial temperature [K]	303
Nitrogen molar concentration [%]	99.9		

* FMOFCu data produced in-house.

Table 2
Physical properties of FMOFCu.

Adsorbent data	Value
Pellet diameter [mm]	0.9*
Solid void fraction	0.080*
Total pore volume (p/p0 = 0.990) [cm^3/g]	0.067*
Mean pore diameter [nm]	5.46*
Solid heat capacity [J/kg • K]	1457**
Solid thermal conductivity [W/m • K]	0.70**

* FMOFCu data produced in-house;
** [38].

amounts of the adsorbed Xe and N_2 were approximately 10 times different (Fig. 3), proving that FMOFCu is a suitable adsorbent for Xe and N_2 separation. Using regression methods, isotherm curves were used to determine the isotherm parameters by fitting them to the Langmuir 2 model equation (Eq.8 in Table A1). The estimated parameters are presented in Table 3. The mass transfer coefficient (MTC) was derived by adapting the work from [39]). The calculated MTC values for xenon and nitrogen are 0.5234 and 1.1184, respectively.

2.4. Parametric study

A parametric study was conducted to identify technically and economically favorable conditions for reaching the target purity. The parametric study was performed considering both process and economic aspects. The study of the process parameters focused on changes in the flow rate, adsorption pressure, and desorption pressure. The electricity price was selected as the economic parameter. These parameters were selected because they were expected to have the most significant effect on the results. Notably, due to very low desorption pressures were used, a parametric study on desorption pressure was conducted to consider the challenges associated with low pressures. All parameter conditions are listed in Table 4.

The product stream from the first-stage can be varied under different parametric conditions. Therefore, adjusting the parameters in the second-stage is necessary to achieve the target. In this study, the bed size was adjusted to accommodate the amount of xenon in each feed.

2.5. Economic and environmental analyses framework

The economic benefit and environmental suitability of the developed xenon recovery process were investigated. For the economic analysis, the minimum selling price (MSP) was calculated based on 2023 USD. The MSP was calculated by annualizing the total capital cost (TCC) and total operating cost (TOC), assuming a 20-year operating period [40–43]. The framework for the economic analysis is shown in Fig. 4. The formula for the MSP is defined in Eqn. (4).

$$MSP = \frac{TCC \times \frac{i(1+i)^n}{(1+i)^n-1} + TOC}{mXe} \quad (4)$$

where i, n, and mXe represent the interest rate (8 % in this study [41]), operating year (20 years), and annualized production based on 7500 operating hours per year [44], respectively.

The total equipment cost (TEC) was derived using Aspen Hysys V11, and an overview of the process designed for Hysys is shown in Fig. C1. The cost of the adsorbent was estimated to be 1135.93 USD/kg. The adsorbent is assumed to be recharged annually. The electricity cost was calculated as 0.12 $/kW [45].

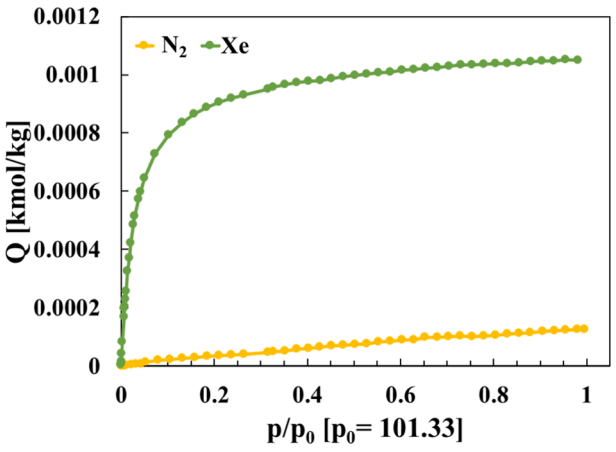

Fig. 3. Isotherms of N_2 and Xe on FMOFCu.

Table 3
Equilibrium isotherms parameters of each component.

Parameter	Nitrogen	Xenon
$q_i b_{0,i}[kJkmol^{-1}K^{-1}]$	0.0012	0.0014
$\frac{-\Delta H_i}{R_g}[K]$	1500	3000
$b_{0,i}[bar^{-1}]$	0.0030	0.0013

Table 4
Parametric study conditions.

Condition	Value
Feed flowrate [kmol/h]	6, 8, 12, 14
Adsorption pressure [bar]	4, 6, 10, 12
Desorption pressure [bar]	0.02, 0.2, 1
Electricity cost [$/kW]	0.06, 0.09, 0.15, 0.18, and 0.21

The environmental impact of the proposed VPSA process was evaluated in terms of the global warming potential (GWP) and environmental cost. The GWP was calculated using Ecoinvent 3.9.1 based on the electricity consumption required to produce 1 kg of xenon [46,47]. For the proposed VPSA process, the electricity consumption was calculated using Aspen HYSYS V11. The calculated GWP was converted using the carbon prices from the Korean emission trading system (ETS) in 2024 to calculate the environmental cost (EC) [48].

3. Result and Discussion

3.1. Results of the first-stage

Parameter studies of the adsorption/desorption pressure and flow rate of the proposed VPSA were performed, and the purity and recovery results for all cases were explored. All simulation results for the first-stage are summarized in Table D1 in Appendix D.

The results of the parametric study of the adsorption pressure are shown in Fig. 5. As shown in Fig. 5(a), both the product purity and recovery improved with an increase in the adsorption pressure. This can be attributed to a higher adsorption pressure causing xenon to be densely adsorbed during the AD step (see Fig. D1) and less xenon breaking through the waste (Fig. 5(b)), thereby leading to greater high-purity desorption in the PU step. As shown in Fig. 5(b), the blowdown recovery increases slightly up to 8 bar and then decreases. As the adsorption pressure increased, the flow rate during blowdown rose, leading to a slight increase in blowdown recovery. However, xenon desorbs effectively at bed pressures below 0.1 bar [24]. When the adsorption pressure exceeded 10 bar, the bed pressure did not reach below 0.1 bar within the 10 s (BD step), resulting in a lower xenon desorption and a significant decrease in blowdown recovery. In addition, as shown in Fig. 5(c), the product flow rate increases with increasing adsorption pressure because of the increase in product purity and recovery. A higher pressure stored more xenon on the adsorbent during the AD step, resulting in a higher purity flow in the PU step.

The desorption pressure is shown in Fig. 6. As shown in Fig. 6(a), increasing the desorption pressure significantly decreases the product purity and recovery. This is due to poor xenon desorption during PU when the desorption pressure is high, resulting in less xenon being recovered as a product. When the desorption pressure is higher than 0.2 bar, a significant amount of xenon remains adsorbed on the adsorbent after the PU step (see Fig. D2 in the Appendix). As a result, the adsorption capacity of adsorbent decreased in the AD step and most of the xenon escaped to the waste stream (Fig. 6(b)). In the BD step, blowdown recovery decreased with an increase in the desorption pressure (Fig. 6(b)) because the pressure difference between the bed and blowdown stream was reduced, which reduced the blowdown flow rate.

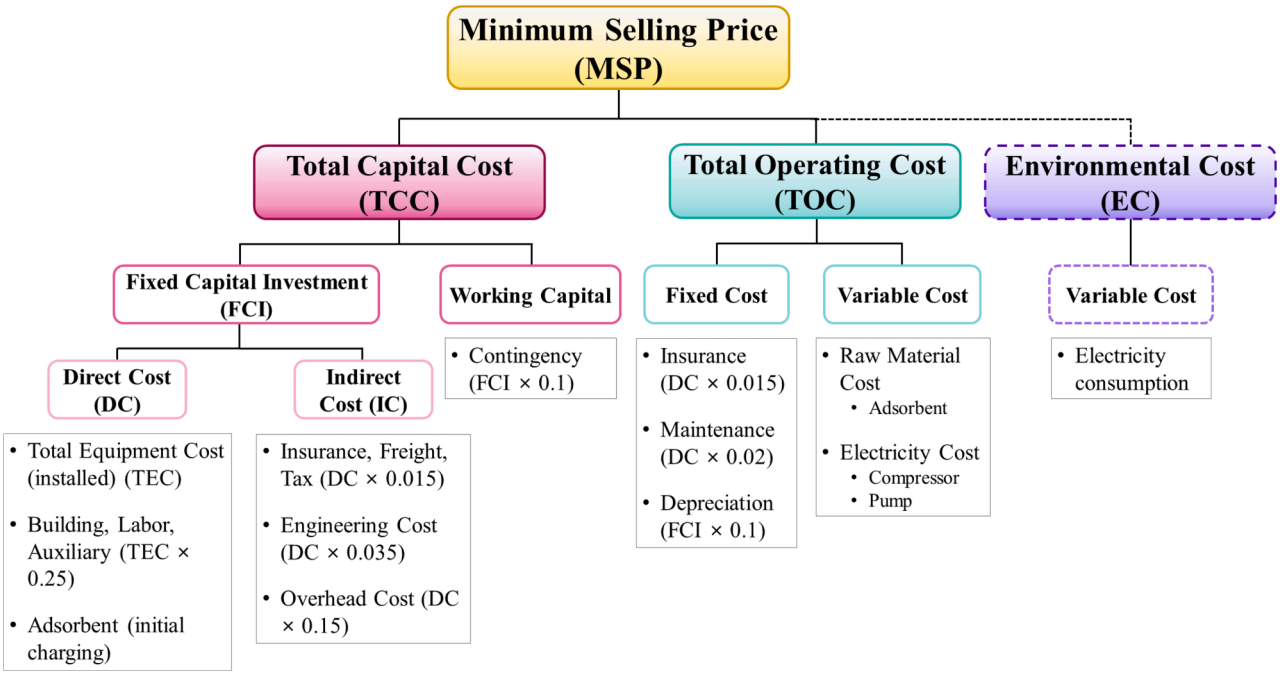

Fig. 4. Economic analysis framework of the Xe recovery process.

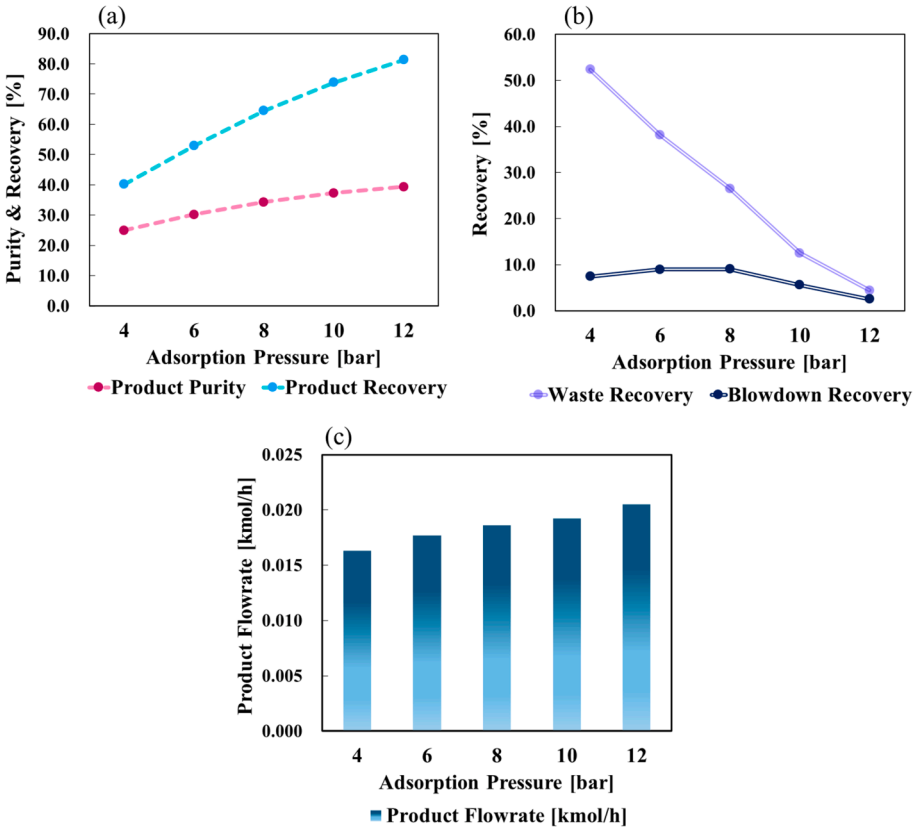

Fig. 5. Results of the adsorption pressure parametric study.

The blowdown recovery was reduced at 0.002 bar. Although the pressure difference between the bed and blowdown stream was large, the volume of the gas at 0.002 bar was substantially large and could not easily pass through the valve, reducing the flow rate. In addition, at a higher desorption pressure, the product flow rate decreased significantly (Fig. 6(c)) because of insufficient desorption.

Furthermore, the product recovery decreased noticeably with an increase in the feed flow rate (Fig. 7(a)) because the bed could not accommodate the increased xenon in the feed, resulting in a greater breakthrough in the bed (see Fig. D3 in Appendix). Consequently, waste recovery increased significantly, as shown in Fig. 7(b). The increased adsorption led to an increase in the product flow rate (Fig. 7(c) and

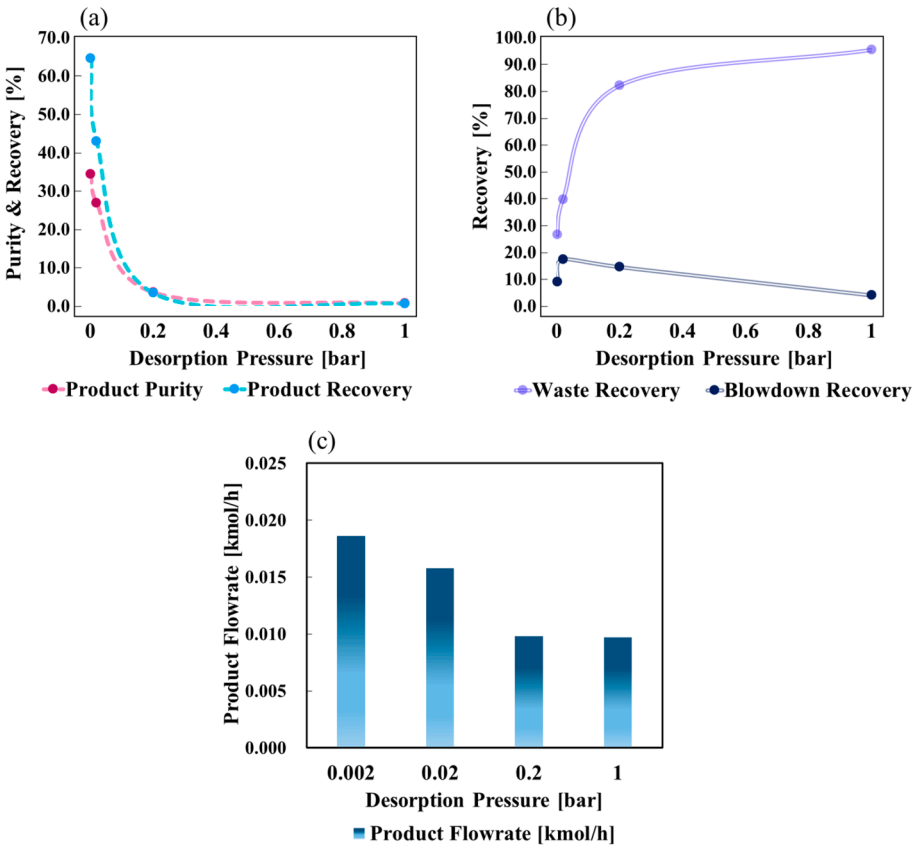

Fig. 6. Results of the desorption pressure parametric study.

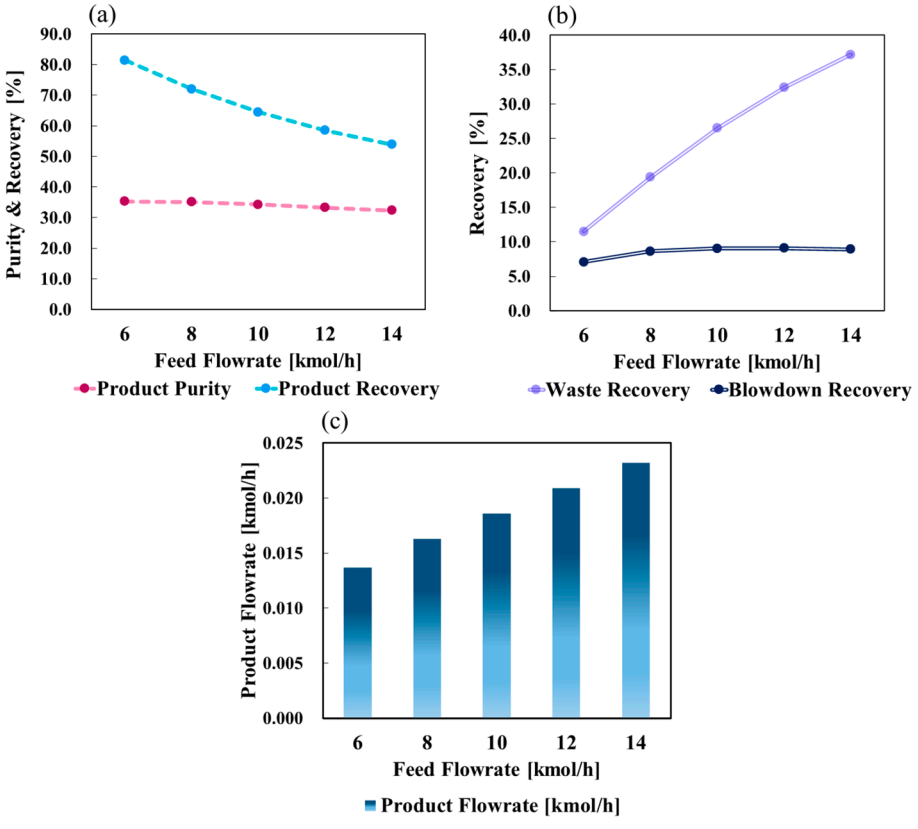

Fig. 7. Results of the product flowrate parametric study.

Fig. D3). In contrast, the product purity decreased slightly (Fig. 7(a)) because the reflux (see (e) in Appendix B) flow rate increased with an increase in the feed flow rate, resulting in a slightly higher nitrogen ratio in the product. Another important point is that a notable pressure drop occurred due to the high flow rate compared to the diameter. However, because of the low concentration of adsorbates in the feed (0.1 %), the pressure drop remained within acceptable levels. The bed pressure along the bed during the AD step is shown in Fig. D4 in Appendix D.

As shown in Fig. 8, a tornado chart was drawn to analyze the impact of each parameter on performance. Negative changes were not considered because the desorption pressure was extremely low (0.002 bar). The tangent represents the rate of performance change with a change in the parameter. Further, as shown in Fig. 8, adsorption pressure had the greater impact on purity. Lowering the adsorption pressure has a greater impact than increasing the pressure. The feed flow rate and desorption pressure had less of an impact on the purity than that of the adsorption pressure. In Fig. 8(a), the desorption pressure seemed to have a large impact owing to the large variation of 5000 %; however, it was the smallest.

Further, the adsorption pressure had the largest impact on recovery. As with purity, the impact was larger when the adsorption pressure decreased than that when it increased. The feed flow rate also had a significant impact on recovery, with a lower feed flow rate having a more favorable impact than a higher feed flow rate. The desorption pressure had a greater impact on recovery than on purity; however, it still had a lower impact than the other parameters.

Overall, each parameter had a greater impact on recovery than that on purity. As the adsorption pressure and feed flow rate had the most significant impact, the second-stage VPSA was designed based on these two parametric studies.

3.2. Results of the second-stage

The second-stage VPSA was performed to produce the product with the target purity (99.9 %) using products from each parametric study cases in the first-stage as the feed. All simulation results for the second-stage VPSA are summarized in Table D2 in the Appendix. In the second-stage VPSA, the target purity could not be achieved using the previous cycle configuration; therefore, the cycle was adjusted, as described in Appendix E. Further, the bed size was adjusted in the second-stage VPSA (Table D2 in the Appendix) because the purity and feed flow rate were significantly different from that for the first-stage VPSA. The target purity was achievable at an adsorption pressure of 2 bar, and therefore, a further increase in the adsorption pressure was not explored because of the unprofitable effects of increased energy consumption and CAPEX. Consequently, the target purity was achieved, and the product recovery exceeded 70 % in all cases. In Table E1 and Fig. E3, the stepwise changes in stream composition and xenon surface coverage in the base case after reaching CSS are shown.

The product flow rate showed a larger difference than those of purity and recovery. The product flow rate increased with an increase in the adsorption pressure and feed flow rate (Fig. 9) because these parameters were positively correlated with the product flow rate in the first- stage VPSA, which increased the feed flow rate in the second-stage VPSA. The increased purity and recovery of the first-stage product positively affected the second-stage product. The best case was the 5–2 case with an adsorption pressure of 12 bar; the worst case was the 2–2 case with an adsorption pressure of 4 bar.

In conclusion, the 5–2 case with an adsorption pressure of 12 bar achieved the best purity and recovery in the first-stage VPSA process. In addition, the 5–2 case had the highest product flow rate in the second-stage VPSA process. Increasing the adsorption pressure was the most effective method for improving the process performance.

3.3. Economic analysis

An economic analysis was performed using the methodology described in Section 2.5. The results are shown in Fig. 10, and the conditions and performance result are listed in Tables F1–F2 of the appendix. The MSP decreased with increasing adsorption pressure and feed flow rate. There was a large difference in the results between the 4 bar and 6 bar cases, and this difference decreased thereafter. MSP decreased with an increase in the feed flow rate. From 2020 to 2023, the market price of xenon ranges from ~ 2,544$/kg to 15,270$/kg [14]. In comparison, the highest MSP calculated for the proposed VPSA process,

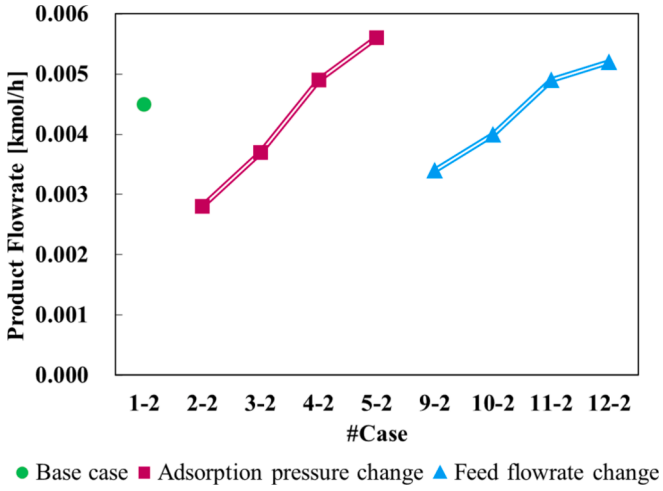

Fig. 9. Change in the product flowrate in the second-stage VPSA process.

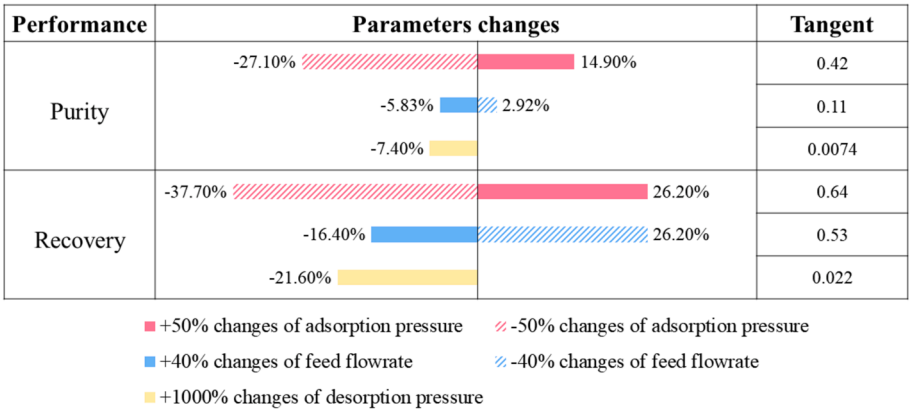

Fig. 8. Tornado chart of purity and recovery in change of parameters.

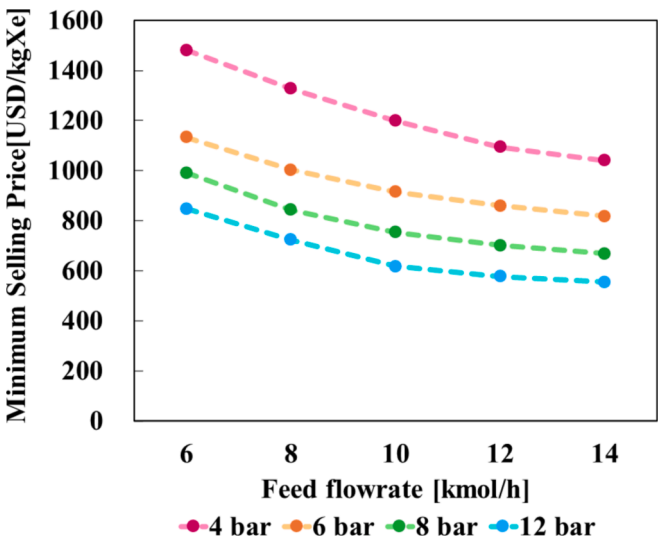

Fig. 10. Minimum selling price for cases with varied adsorption pressures and feed flowrates.

with an adsorption pressure of 4 bar and a feed flow rate of 6 kmol/h, was ~$1,500/kg, which is significantly cheaper.

A detailed breakdown of the MSP in the proposed VPSA process is presented in Fig. 11. As shown in Fig. 11 (a), TCC and TOC contributed similarly, with TCC contributing slightly more. As shown in Fig. 4, TEC is the main contributor to MSP, and therefore, it is analyzed in detail in Fig. 11(b). The largest cost in the TEC was that of the compressor, accounting for ~ 82 %. Although the price of the compressor was the most influential, the higher the adsorption pressure, the lower was the MSP. This implies that the economic benefits of increasing xenon recovery outweigh the capital and operating costs of increasing pressure. Depreciation accounted for the largest share of the TOC, which was primarily influenced by TEC. In contrast, the raw material and electricity costs constituted a minor share of the TOC because there was no feed cost attributable to the recycling of waste gas, and only the adsorbent cost was required. In addition, the electricity consumption per 1 kg xenon produced by the traditional process was 1400.97 kWh [46], whereas that produced by the proposed VPSA process was 40.99 kWh, which is 34 times lower.

3.4. Environmental analysis

An environmental analysis was performed using the methodology described in Section 2.5. The environmental analysis of traditional xenon production was performed to compare the environmental impact of the current xenon production process with that of the proposed VPSA process. The results are summarized in Table 5.

As shown in Table 5, the power consumption of the proposed VPSA process is only 2.9 % of that of the traditional process, which is remarkably low. The GWP of the proposed VPSA process is also very low at 2.6 % of that of the traditional process. However, the impact of the GWP on the MSP is negligible because of the low carbon prices in Korea.

3.5. Discussion

The proposed VPSA system was analyzed to determine its competitiveness with other xenon production methods. The data are summarized in Table 6, which compares the VPSA system with other processes such as gas hydrate formation, cryogenic distillation, membrane separation, and batch distillation. Producing xenon is challenging especially when starting with a low-concentration feed (1 percent or less), and therefore, complex hybrid processes that can operate under extreme conditions are required. Moreover, economic and environmental analyses of the xenon production process are not included in Table 6 because none of the studies provided data.

Compared to the traditional process, the proposed VPSA process requires significantly less electricity and operates at room temperature. Unlike traditional processes, the proposed VPSA process cannot purify xenon from the atmosphere; however, it can purify concentrations as low as 0.1 mol%. Further, the VPSA system produces xenon with 99.9 % purity, making it suitable for practical use. In addition, recycling semiconductor waste gas, which has a xenon concentration over 10,000 times higher than that of xenon in air, reduces energy consumption for enrichment.

The hybrid process of gas hydration and cryogenic distillation [15] uses by-product gas from the ASU to purify Xe, allowing them to use a feed with a relatively high xenon concentration of 25.7 % to produce a product with 99.9 % xenon purity. However, the hybrid process requires

Table 5
Environmental analysis results of the traditional and proposed VPSA processes.

Data	Traditional process	VPSA process
Electricity consumption [kWh/kg Xe]	1400.97*	40.99
GWP [kg CO_2 eq]	1104.99*	28.92**
Carbon prices in Korean ETS [$/kg CO_2]	0.00678***	0.00018***
MSP [$/kg CO_2]	2544	753.58
MSP + Carbon prices [$/kg CO_2]	2551	754

* Ecoinvent [46];
** GWP of Korea Electricity from Ecoinvent [46];
*** ICAP-Korean ETS 2023[48].

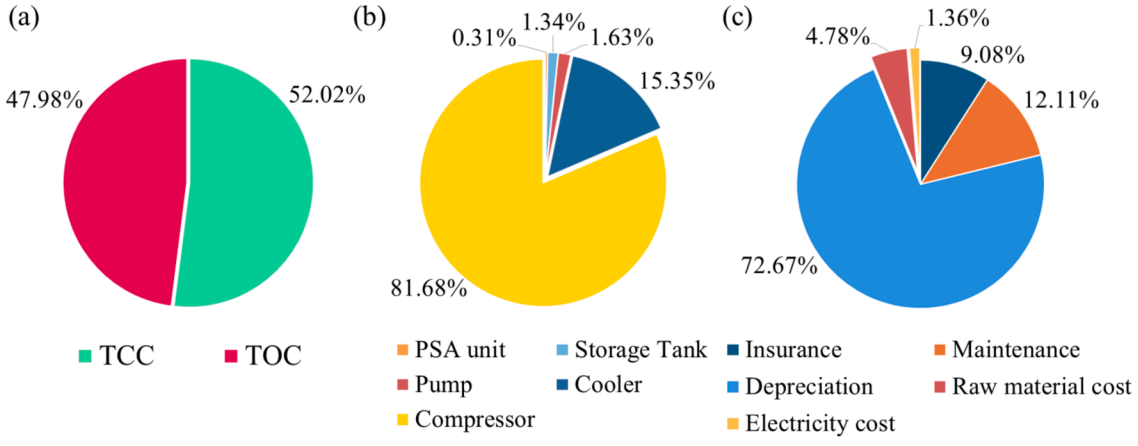

Fig. 11. (a) MSP breakdown (b) TEC breakdown, and (c) TOC breakdown.

Table 6
Comparison of the xenon production process.

Process description	Feed	Pressure/ Temperature	Electricity consumption*	Product purity	References
Proposed VPSA process	Xe 0.1 mol%	0.002–12 bar/303 K	2.43 kWh/kmol	99.9 %	This study
Traditional process (ASU)	Xe 0.000009 mol%	0.3–0.5 bar/165 K	9.8 kWh/kmol	99.999 %	[10]
Gas Hydrate and cryogenic distillation	Xe 25.7 mol%	20.6 bar/272 K	3.5 kWh/kmol	99.99 %	[15]
Gas hydrate crystallization and membrane process	Xe 0.15 mol%	1–60 bar/253–313 K	2617 kWh/kmol**	99.96 mol%***	[16]
Batch distillation and membrane process	Xe 0.15 mol%****	1–20 bar/165–243 K	3112–3123 kWh/kmol****	99.9999 %	[17]
Membranes separation	Xe 20 mol%	150 bar/243 K	7.9 kWh/kmol	Xe: 99.93 mol% Kr: 99.6 mol%	[18]

* Electricity consumption per kilomole of feed;
** Calculated using information provided in the literature;
*** Data calculated or derived from the results of [17];
**** Electricity consumption required to produce xenon in concentrations from 0.15 to 99.96% is derived from the work of [16], total electricity consumption required to produce xenon at a concentration of 99.9999% with 0.15%.

a high pressure of 20.6 bar and 44 % more electricity than that required by the proposed VPSA process, which suggests that the proposed VPSA process is more energy efficient process for xenon separation.

A hybrid process of hydrate crystallization [16] and membrane processes has been used to recover xenon from natural gas. The feed gas of the hybrid process has a xenon concentration similar to that of the semiconductor waste gas; however, it requires very high pressure and relatively low temperatures to form hydrates. The hybrid process consumed 1,000 times more electricity than the proposed VPSA process, even without including xenon separation from the formed hydrates.

Hybrid batch distillation and membrane process [17] have also been used to produce xenon from natural gas. A xenon feed with 99.96 % purity obtained through gas hydrate crystallization was used to produce 6 N and 9 N pure Xe. Since the hybrid process operates under high pressure and low temperature conditions, a significant amount of electricity was required.

Membrane separation [18] utilizes the by-products of ASU. Even when starting from a relatively high concentration of 20 % xenon feed, the membrane process used 325 % more electricity than the proposed VPSA process. Furthermore, the membrane process was operated under extreme pressure and relatively low-temperature conditions. In contrast, the proposed VPSA process was operated not only at room temperature but also at only 10 % of the pressure required by the membrane process.

To enable valid comparisons, an investigation was conducted to identify membrane separation processes utilizing feed streams with less than 1 % xenon. While there are examples of using direct air capture (DAC) to separate other components such as CO_2, there are no documented cases of separating xenon, so the paper using a 20 % xenon feed was referenced. The need for high pressure should be considered when using lower concentrations of feed, as higher feed concentrations typically provide sufficient driving force for separation across the membrane. Therefore, the energy consumption of the membrane separation process is expected to increase when using a low concentration of xenon feed, as in the other examples.

Most xenon separation processes operate at high pressures and low temperatures, thereby requiring more energy than that of the proposed VPSA. Thus, xenon enrichment using semiconductor waste gas appears to have an advantage over other xenon enrichment processes in terms of energy consumption.

4. Conclusion

A VPSA process was proposed for xenon separation to produce xenon in a more economical and environmentally friendly manner. The MSP of xenon in the base case was $753.58/kg, with the lowest MSP at $554.41/kg for the 14 kmol/h feed flow rate case with an adsorption pressure of 12 bar. This is less than 30 % of the lowest price in the recent xenon market, indicating that xenon produced by the proposed VPSA system is economically viable. Further, the proposed VPSA system consumes 75 % less electricity than the traditional xenon production process to produce the same amount of Xe. Carbon emissions can be reduced by consuming less electricity, making the proposed VPSA system more environmentally friendly than the conventional processes.

Furthermore, compared to the various xenon separation processes currently being studied, the proposed VPSA system uses considerably less electricity and has milder process conditions. Therefore, xenon separation for recycling semiconductor waste gas is an economically and environmentally promising approach for xenon production. However, research covering the economic and environmental analyses of xenon production processes remains lacking, and thus, further research on the MSP and the life cycle assessment of various xenon production processes would be valuable.

CRediT authorship contribution statement

YeonJi Choi: Writing – original draft, Writing – review & editing, Methodology, Data curation, Software. **Kyung Min Choi:** Conceptualization, Funding acquisition. **Kyungtae Park:** Conceptualization, Writing – review & editing, Methodology, Supervision, Funding acquisition.

Funding

This work was supported by the Korea Technology and Information Promotion Agency for SMEs (TIPA) grant funded by the Korea Government (MSS) [grant number: RS-2023–00217429, Development of adsorption technology and selective adsorbent for special gases (ultra-high purity hydrogen fluoride (HF), Xe, Kr) used for semiconductor etching and ion implantation processes].

Declaration of competing interest

The authors declare that they have no known competing financial interests or personal relationships that could have appeared to influence the work reported in this paper.

Appendix A. . Governing equations of the model

.

Table A1
Governing equations used in the model.

Model equation	Expression	
Mass balance	$\varepsilon\frac{\partial(w_i\rho_T)}{\partial t} = -\frac{\partial(w_i\rho_T v_{sup})}{\partial z} + \varepsilon_{bed}\frac{\partial}{\partial z}\left(D\rho_T\frac{\partial w_i}{\partial z}\right) - N_{ads-mass,i}$	(1*)
Energy balance	Fluid phase $\frac{\partial \widehat{U}_{bed}}{\partial t} = \varepsilon_{bed}\frac{\partial}{\partial z}\left(\rho_T D\frac{\partial H_f}{\partial z}\right) - \frac{\partial(v_{sup}\rho H_f)}{\partial z} + \frac{1}{1000}\frac{\partial}{\partial z}\left(\lambda_{eff}\frac{\partial T_f}{\partial z}\right) - \frac{4}{d_{bed}}\frac{1}{1000}h_{f-w}(T_f - T_w)$	(2*)
	Adsorbed phase $\widehat{U}_{bed} = \varepsilon(\rho_T H_f - 10^2 P) + \rho_{bed}\left(\sum_C \overline{q}_i \widetilde{H}_{ads,i}|_{T_f} + C_{p,solid}(T_f - T_{ref,solid})\right)$	(3*)
	Bed wall $\rho_w C_{p,w}\frac{\partial T_w}{\partial t} = \frac{\partial}{\partial z}\left(\lambda_w\frac{\partial T_w}{\partial z}\right) + h_{f-w}\frac{d_{bed}}{\left(\frac{d_{bed}}{2}+l_w\right)^2 - \left(\frac{d_{bed}}{2}\right)^2}(T_f - T_w) + h_{w-a}\frac{(d_{bed}+2l_w)}{\left(\frac{d_{bed}}{2}+l_w\right)^2 - \left(\frac{d_{bed}}{2}\right)^2}(T_a - T_w)$	(4*)
Momentum balance	$-\frac{\partial P}{\partial z} - 150\mu\frac{(1-\varepsilon_{bed})^2 v_{sup}}{\varepsilon_{bed}{}^3 d_{pellet}{}^2} - \frac{1.75(1-\varepsilon_{bed})\rho_T v_{sup}{}^2}{\varepsilon_{bed}{}^3 d_{pellet}} = 0$	(5*)
Mass transfer rate	$\frac{\partial \overline{q_i}}{\partial t} = k_c\left(\overline{q_i^*}|_{C_i} - \overline{q_i}\right)$	(6*)
Mass transfer coefficient	$\frac{\partial Q_i}{\partial t} = \frac{15 D_{e,i}}{R_p^2}(Q_i^* - Q_i)$	(7**)
Equilibrium isotherm	$q^* = \frac{\left(q_i b_{0,i} exp\left(\frac{-\Delta H_i}{R_g T_s}\right)\right)P}{1 + \left(b_{0,i} exp\left(\frac{-\Delta H_i}{R_g T_s}\right)\right)P}$	(8***)

*[49], **[39], ***[50].

Appendix B. . Cycle description

(a) Adsorption (AD): Components with high affinity for the adsorbent are selectively stored when the high-pressure feed flows through the adsorption bed. The AD step is connected to the beds of the other PU and PR steps for some time, and a portion of the discharged gas (waste gas) is used as the purging gas for the PU step and pressurization gas for the PR step.
(b) Idle step (ID): The bed is idle and has no connection to any other bed or stream. This step is introduced between steps to synchronize the interaction times with the other beds in the next step.
(c) Pressure equalization (depressurization) (ED): The ED step-bed is connected to the ER step-bed using an intermediate valve to achieve pressure equilibrium. In this step, the pressure is partially reduced before the BD step to reduce the mechanical energy consumption [51] and prevent sudden pressure changes, which can possibly affect the adsorbent durability.
(d) Blowdown (BD): Before the PU step, the bed is blown down to ensure sufficient vacuum pressure for the PU step.
(e) Desorption (purging) (PU): The stored components are desorbed from the PU bed at a low pressure, and a high-purity xenon product gas is produced. Part of the exhaust gas from the AD step-bed is used as reflux to facilitate desorption. The adsorption bed is regenerated and prepared for the subsequent AD steps.
(f) Pressure equalization (re-pressurization) (ER): In contrast to the ED step, the ER step is pressurized through pressure equilibrium. Likewise, it prevents dramatic pressure changes and reduces mechanical energy consumption.
(g) Re-pressurization (PR): The PR step bed is re-pressurized using exhausted gas at the end of the AD step. Because such gases contain relatively high amounts of unadsorbed Xe, the reflux can be used to increase recovery.

Appendix C. . Xenon separation unit

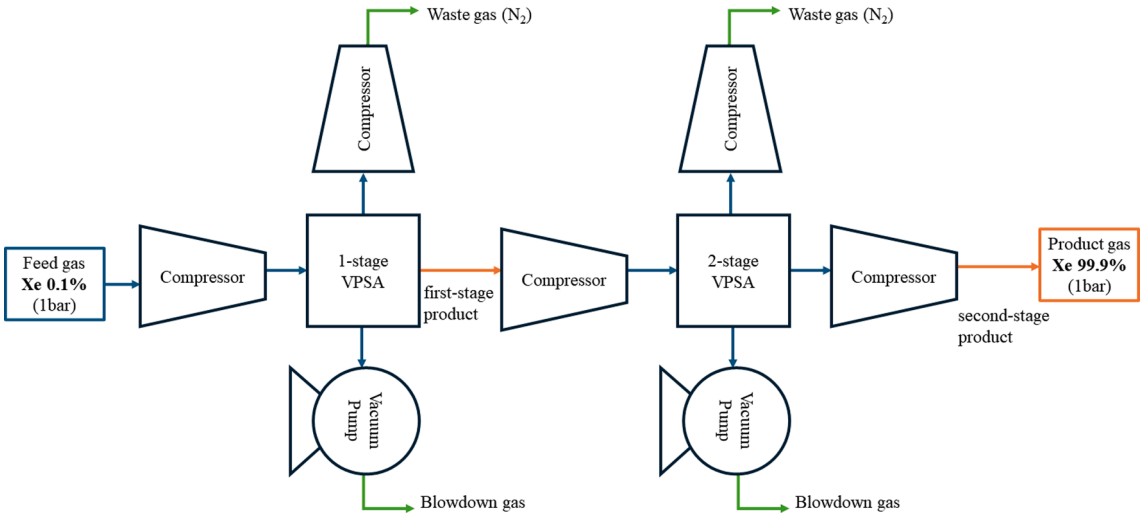

Fig. C1. Graphical overview of the xenon separation unit

Appendix D. . Simulation result

The simulation results for all cases are summarized in this section. All simulation results presented in this section reached the cyclic steady state according to the criteria mentioned in Section 2.3.1.

The first- and second- stage VPSA had t_{cycle} values of 800 and 840 s, respectively. Therefore, the number of cycles operated in a year (n_{cycle}) was ~ 33750 for the first- stage and 32,143 for the second- stage (based on 7500 operating hours).

Table D1
First-stage VPSA process simulation results.

Case#	P_{AD} [bar]	P_{PU} [bar]	F_{feed} [kmol/h]	Xe purity (product) [%]	Xe recovery (product) [%]	Xe recovery (Waste) [%]	Xe recovery (Blowdown)[%]	F_{prod} [kmol/h]
1–1*	8	0.002	10	34.3	64.5	26.5	9.02	0.0186
2–1	4	0.002	10	25.0	40.2	52.4	7.46	0.0163
3–1	6	0.002	10	30.2	52.9	38.1	8.98	0.0177
4–1	10	0.002	10	37.3	73.9	12.5	5.57	0.0192
5–1	12	0.002	10	39.4	81.4	4.40	2.50	0.0205
6–1	8	0.02	10	26.9	42.9	39.7	17.4	0.0158
7–1	8	0.2	10	3.54	3.46	82.0	14.6	0.0098
8–1	8	1	10	0.645	0.628	95.4	3.99	0.0097
9–1	8	0.002	6	35.3	81.4	11.5	7.08	0.0137
10–1	8	0.002	8	35.1	72.0	19.4	8.64	0.0163
11–1	8	0.002	12	33.3	58.5	32.4	9.08	0.0209
12–1	8	0.002	14	32.3	53.9	37.2	8.92	0.0232

* Base case; Cases 2–1 to 5–1: adsorption pressure parametric study; Cases 6–1 to 8–1: desorption pressure parametric study; Cases 9–1 to 12–1: feed flow rate parametric study.

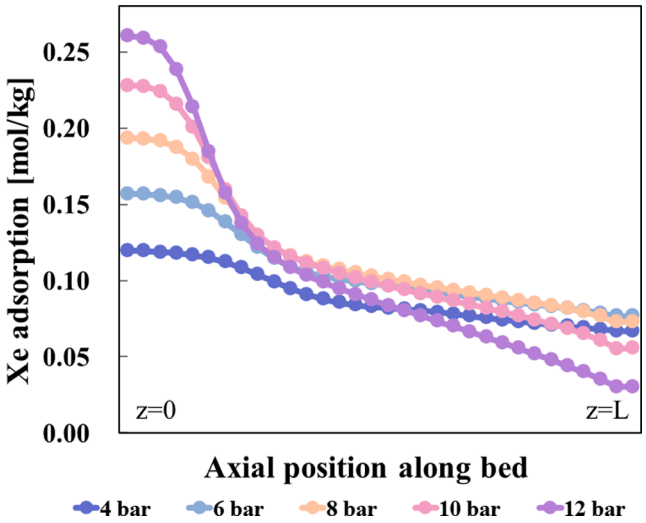

Fig. D1. Change in the adsorption front caused by the varied adsorption pressure after the AD step (The feed inlet position of the bed: z = 0, the waste and blowdown outlet position: z = L).

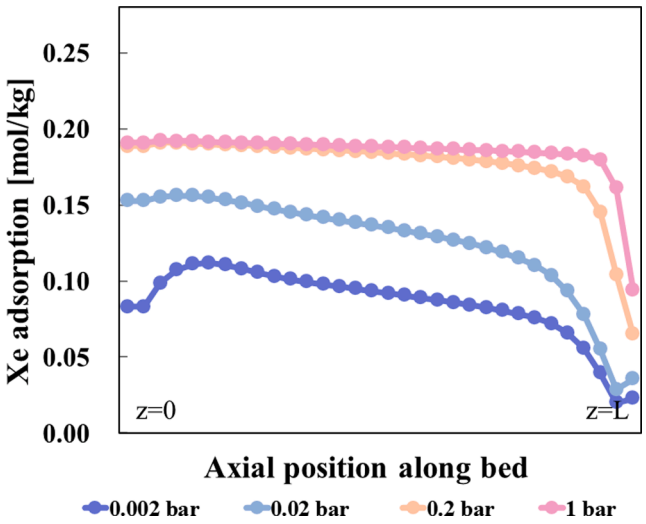

Fig. D2. Change in the adsorption front caused by the varied desorption pressure after the PU step (The feed inlet position of the bed: z = 0, the waste and blowdown outlet position: z = L).

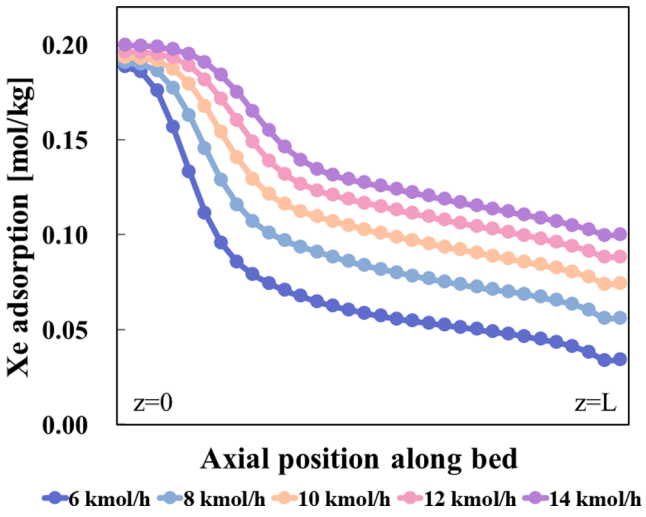

Fig. D3. Change in the adsorption front caused by the varied feed flowrate after the AD step (The feed inlet position of the bed: z = 0, the waste and blowdown outlet position: z = L).

Table D2
Second-stage VPSA process parametric study conditions and results.

Case#	Bed length [m]	Bed diameter [m]	F_{feed} [kmol/h]	Xe purity (product) [%]	Xe recovery (product) [%]	Xe recovery (Waste) [%]	Xe recovery (Blowdown) [%]	F_{prod} [kmol/h]
1–2	0.7	0.07	0.0186	99.9	74.9	0.951	24.0	0.0045
2–2	0.6	0.06	0.0163	99.9	74.4	1.72	23.6	0.0028
3–2	0.65	0.065	0.0177	99.9	74.2	1.25	24.3	0.0037
4–2	0.7	0.07	0.0192	99.9	74.4	0.847	24.6	0.0049
5–2	0.7	0.07	0.0205	99.9	72.2	0.844	26.9	0.0056
9–2	0.6	0.06	0.0137	99.9	72.9	1.00	26.0	0.0034
10–2	0.65	0.065	0.0163	99.9	73.7	0.953	25.2	0.0040
11–2	0.7	0.07	0.0209	99.9	74.1	1.09	24.6	0.0049
12–2	0.75	0.075	0.0232	99.9	73.1	1.22	25.5	0.0052

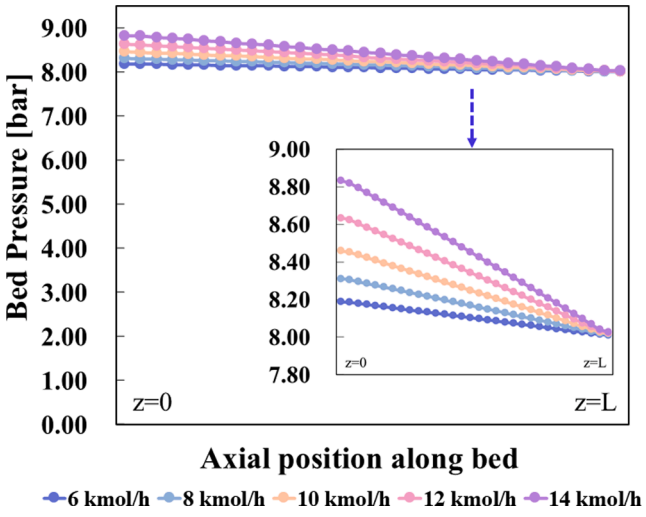

Fig. D4. Change of the bed pressure along the bed axial position

Appendix E. . Second-stage cycle configuration

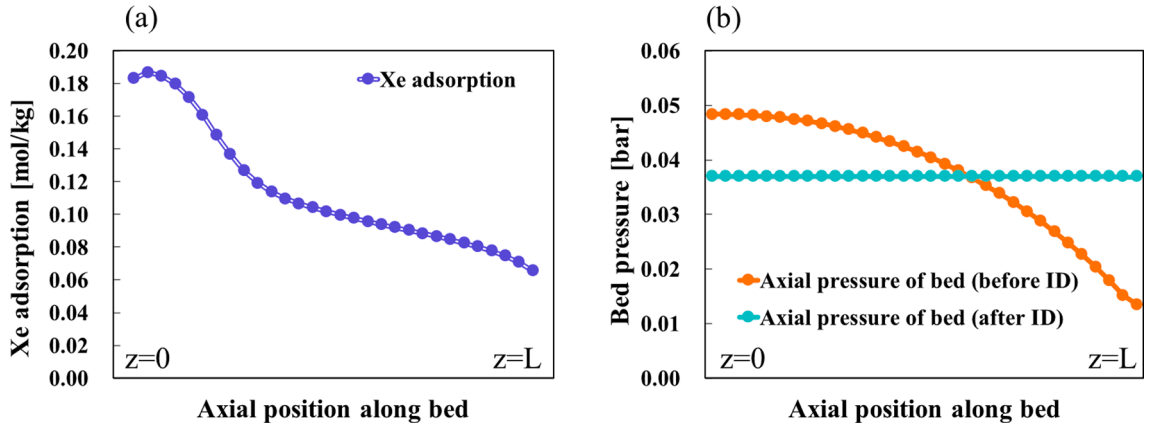

Fig. E1. (a) Adsorption front after the AD step. (b) Bed pressure of the ID step before and after (The feed inlet position of the bed: z = 0, the waste and blowdown outlet position: z = L).

As shown in Fig. E1 (a), the adsorption of xenon is concentrated near z = 0. Therefore, proper pressure drops at z = 0 are key for xenon desorption to increase product purity and recovery. In Fig. E1 (b), the bed pressure near z = 0 did not decrease compared to the pressure near z = L (orange curve). Therefore, for the axial equalization of the bed pressure, the ID step was relocated shortly after the BD step in the second-stage VPSA. With the modified cycle, the bed pressure profile changed, as shown by the green curve in Fig. E1 (b), and the target purity was reached. The modified cycle for the second-stage VPSA is shown in Fig. E2.

Step	Step 1			Step 2	Step 3	Step 4			Step 5	Step 6	Step 7	Step 8
Time(s)	210			10	30	210			170	10	30	170
Bed 1	AD			ED	BD	ID			PU	ER	PR	ID
Bed 2	ER	PR	ID	AD		ED	BD		ID			PU
Bed 3	ID		PU	ER	PR	ID	AD			ED	BD	ID
Bed 4	ED	BD	ID			PU	ER	PR	ID	AD		

Fig. E2. Step sequence and duration of the second-stage VPSA process

Table E1
Xenon composition in streams at the end of each step of second stage VPSA process.

	Feed (AD)	Product (PU)	Blowdown (BD)	Waste (AD)
Composition (%)	Xe 34.29 N_2 65.71	Xe 99.96 N_2 0.04	Xe 99.75 N_2 0.25	Xe 0.76 N_2 99.24

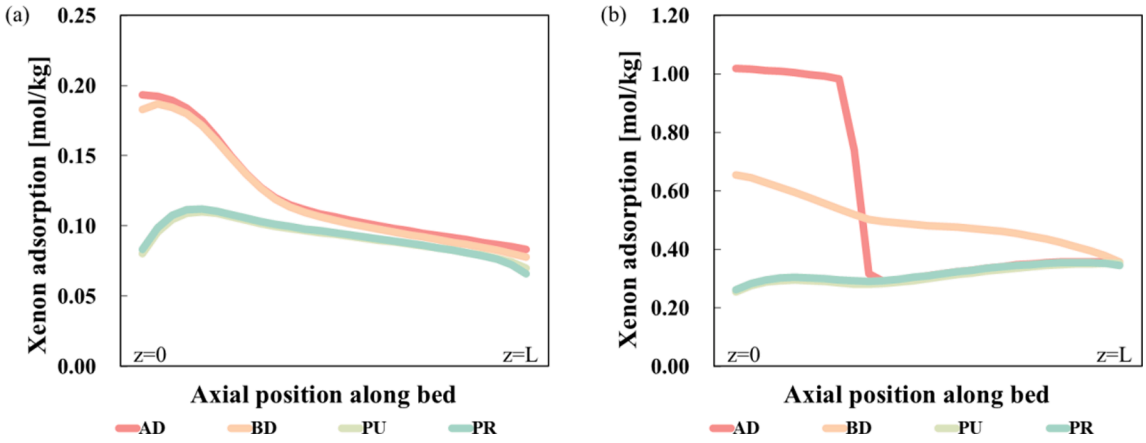

Fig. E3. Amount of xenon adsorption in the bed at the end of the step: (a) first stage (b) second stage

The amount of xenon adsorbed on the bed at the end of the main step (AD-BD-PU-PR) is shown in Fig. E3. Although the cycle configurations of the two stages are slightly different, the change in xenon adsorption along the bed during the main step revealed a similar trend: feed gas was injected at z = 0 during the AD step, leading to xenon adsorption that concentrated at z = 0. In the BD step, a flow towards z = L caused some desorption of xenon. In the second stage BD step (see Fig. E.3 (b)) a relatively large amount of xenon was desorbed as a larger amount had been adsorbed. Consequently, a flow to z = L distributed the xenon towards z = L. In the PU step, a considerable amount of xenon was desorbed at x = 0 as the product was produced towards z = 0. In the PR step, there was little change in the amount of adsorption.

Appendix F. . Simulation results of the economic and environmental analysis

.

Table F1
Results for EA (First-stage VPSA).

Case#	P_{AD} [bar]	P_{PU} [bar]	F_{feed} [kmol/h]	Xe purity (product)	Xe recovery (product)	F_{prod} [kmol/h]
13–1	6	0.002	6	31.44	69.29	0.0131
14–1	6	0.002	8	30.70	59.67	0.0155
3–1	6	0.002	10	30.24	52.95	0.0177
15–1	6	0.002	12	28.71	47.84	0.0199
16–1	6	0.002	14	27.86	44.15	0.0221
9–1	8	0.002	6	35.28	81.42	0.0137
10–1	8	0.002	8	35.12	72.01	0.0163
1–1	8	0.002	10	34.29	64.46	0.0186

(*continued on next page*)

Table F1 (*continued*)

Case#	P_{AD} [bar]	P_{PU} [bar]	F_{feed} [kmol/h]	Xe purity (product)	Xe recovery (product)	F_{prod} [kmol/h]
11–1	8	0.002	12	33.30	58.54	0.0209
12–1	8	0.002	14	32.31	53.90	0.0232
17–1	12	0.002	6	38.21	94.16	0.0146
18–1	12	0.002	8	39.50	87.84	0.0176
5–1	12	0.002	10	39.39	81.49	0.0205
19–1	12	0.002	12	38.92	75.47	0.0231
20–1	12	0.002	14	37.79	70.10	0.0258

Table F2
Result for EA (second-stage VPSA).

Case#	Bed Length [m]	Bed diameter [m]	F_{feed} [kmol/h]	Xe purity (product)	Xe recovery (product)	F_{prod} [kmol/h]
13–2	0.6	0.06	0.0131	99.9	74.71	0.0029
14–2	0.65	0.065	0.0155	99.9	74.71	0.0034
3–2	0.65	0.065	0.0177	99.9	74.23	0.0037
15–2	0.65	0.065	0.0199	99.9	73.32	0.0040
16–2	0.65	0.065	0.0221	99.9	72.11	0.0042
9–2	0.6	0.06	0.0137	99.9	72.86	0.0034
10–2	0.65	0.065	0.0163	99.9	73.74	0.0040
1–2	0.7	0.07	0.0186	99.9	74.90	0.0045
11–2	0.7	0.07	0.0209	99.9	74.14	0.0049
12–2	0.75	0.075	0.0232	99.9	73.09	0.0052
17–2	0.65	0.065	0.0146	99.9	74.13	0.0039
18–2	0.65	0.065	0.0176	99.9	70.13	0.0047
5–2	0.7	0.07	0.0205	99.9	72.17	0.0056
19–2	0.7	0.07	0.0231	99.9	69.61	0.0060
20–2	0.7	0.07	0.0258	99.9	67.21	0.0063

Data availability

Data will be made available on request.

References

[1] A.E. Neice, M.H. Zornow, Xenon anaesthesia for all, or only a select few? Anaesthesia 71 (2016) 1267–1272, https://doi.org/10.1111/anae.13569.
[2] azooptics, Xenon excimer laser – Properties and applications, Azooptics (2013). https://www.azooptics.com/Article.aspx?ArticleID=484. (accessed August 27, 2024).
[3] R. Gill, E. Bush, P. Haueter, P. Loutzenhiser, Characterization of a 6 kW high-flux solar simulator with an array of xenon arc lamps capable of concentrations of nearly 5000 suns, Rev Sci Instrum (2024).
[4] J. Hansen, D. McDowell, H. Bryan, A. Welty, M. Kropp, M. Fujimoto, B. Riley, Cost-Benefit Assessment of Krypton and Xenon Recovery from Aqueous Reprocessing, 2023. Doi: 10.2172/2377416.
[5] Air Products, Xenon The star of rare gases, AIR Prod. (2024). https://www.airproducts.com/gases/xenon (accessed August 27, 2024).
[6] Global Market Insights, Xenon Gas Market - By Purity (High Purity and Low Purity), By End Use (Healthcare, Automotive, Aerospace and Defense, Electronics and Semiconductors, Research Institutions) & Forecast, 2024 – 2032, Glob. Mark. Insight (2023). https://www.gminsights.com/industry-analysis/xenon-gas-market (accessed August 27, 2024).
[7] V.L. Bondarenko, I.A. Losyakov, O.V. Diachenko, Economic aspects of krypton and xenon production technology, Chem. Pet. Eng. 56 (2020) 263–271, https://doi.org/10.1007/s10556-020-00768-x.
[8] Persistence market research company, Xenon gas market, https://www.persistencemarketresearch.com/market-research/xenon-gas-market.asp (accessed August 27, 2024).
[9] Richard Betzendahl, Ever changing rare gas market, *CryoGas Int.* 32–34. https://www.gasworld.com/feature/ever-changing-rare-gas-market/2078375.article/.
[10] F.G. Kerry, Industrial gas handbook: gas separation and purification, CRC Press, 2007.
[11] M.A. Hnatow, J. Happel, Process and apparatus for separation of constituents of gases using gas hydrates, US 5434330 A, 1993.
[12] R. Welle, Availability considerations in the selection of inert propellants for ion engines, 21st Int Electr. Propuls. Conf. 2589 (2012) 2024, https://doi.org/10.2514/6.1990-2589 (accessed August 27.
[13] A. Gabrielle, A. Gregory, Russia's Invasion of Ukraine Impacts Gas Markets Critical to Chip Production, CSISCenter Strateg. Int. Stud. (2022). https://www.csis.org/blogs/perspectives-innovation/russias-invasion-ukraine-impacts-gas-markets-critical-chip-production (accessed August 27, 2024).
[14] The Economist, How rare-gas supply adapted to Russia's war, Mint (2023). https://www.livemint.com/industry/manufacturing/how-rare-gas-supply-adapted-to-russia-s-war/amp-11690785072859.html. (accessed June 23, 2024).
[15] F. Matizakurima, S. Babaee, H. Hashemi, P. Naidoo, Separation of xenon from noble gas mixtures of argon, krypton, and xenon using gas hydrate technology, Ind. Eng. Chem. Res. 62 (2023) 14484–14496, https://doi.org/10.1021/acs.iecr.3c01174.
[16] M.S. Sergeeva, N.A. Mokhnachev, D.N. Shablykin, A.V. Vorotyntsev, D.M. Zarubin, A.A. Atlaskin, M.M. Trubyanov, I.V. Vorotyntsev, V.M. Vorotyntsev, A. N. Petukhov, Xenon recovery from natural gas by hybrid method based on gas hydrate crystallisation and membrane gas separation, J. Nat. Gas Sci. Eng. 86 (2021) 103740, https://doi.org/10.1016/j.jngse.2020.103740.
[17] A.N. Petukhov, D.N. Shablykin, M.M. Trubyanov, A.A. Atlaskin, D.M. Zarubin, A. V. Vorotyntsev, E.A. Stepanova, K.A. Smorodin, O.V. Kazarina, A.N. Petukhova, V. M. Vorotyntsev, I.V. Vorotynstev, A hybrid batch distillation/membrane process for high purification part 2: Removing of heavy impurities from xenon extracted from natural gas, Sep. Purif. Technol. 294 (2022) 121230, https://doi.org/10.1016/j.seppur.2022.121230.
[18] E.S. Miandoab, S.H. Mousavi, S.E. Kentish, C.A. Scholes, Xenon and krypton separation by membranes at sub-ambient temperatures and its comparison with cryogenic distillation, Sep. Purif. Technol. 262 (2021) 118349, https://doi.org/10.1016/j.seppur.2021.118349.
[19] D.D. Duong, Adsorption Science and Technology, World Scientific Publishing Company, 2000.
[20] M. Yoshida, J.A. Ritter, A. Kodama, M. Goto, T. Hirose, Simulation of an enriching reflux PSA process with parallel equalization for concentrating a trace component in air, Ind. Eng. Chem. Res. 45 (2006) 6243–6250, https://doi.org/10.1021/ie0604573.
[21] R.M. Williams, Extraction of xenon using enriching reflux pressure swing adsorption, Pacific Northwest National Laboratory, DTIC, 2010.
[22] W.R. Schell, J. Vives-Battle, S.R. Yoon, M.J. Tobin, High-pressure swing system for measurements of radioactive fission gases in air samples, Nucl. Instrum. Methods Phys. Res. Sect. Accel. Spectrometers Detect. Assoc. Equip. 420 (1999) 416–428, https://doi.org/10.1016/S0168-9002(98)00646-9.
[23] M. Yamawaki, T. Urakami, Y. Ishihara, Y. Shirai, A. Teramoto, T. Ohmi, Development of a Xenon recycling and supply system for plasma process, in: 2007 Int. Symp. Semicond. Manuf., IEEE, Santa Clara, CA, USA, 2007: pp. 1–4. Doi: 10.1109/ISSM.2007.4446797.
[24] A.D. Johnson, R.V. Pearce, T. Stephen, (54) Recovering of Xenon By Adsorption, US 8535414 B2, 2013.

[25] D. Banerjee, C.M. Simon, S.K. Elsaidi, M. Haranczyk, P.K. Thallapally, Xenon gas separation and storage using metal-organic frameworks, Chem 4 (2018) 466–494, https://doi.org/10.1016/j.chempr.2017.12.025.
[26] S. Sircar, Pressure swing adsorption, Ind. Eng. Chem. Res. 41 (2002) 1389–1392, https://doi.org/10.1021/ie0109758.
[27] A. Ali Abd, M. Roslee Othman, Biogas upgrading to fuel grade methane using pressure swing adsorption: Parametric sensitivity analysis on an industrial scale, Fuel 308 (2022) 121986, https://doi.org/10.1016/j.fuel.2021.121986.
[28] J. Chicano, C.T. Dion, U. Pasaogullari, J.A. Valla, Simulation of 12-bed vacuum pressure-swing adsorption for hydrogen separation from methanol-steam reforming off-gas, Int. J. Hydrog. Energy 46 (2021) 28626–28640, https://doi.org/10.1016/j.ijhydene.2021.06.102.
[29] Q. Fu, H. Yan, Y. Shen, Y. Qin, D. Zhang, Y. Zhou, Optimal design and control of pressure swing adsorption process for N2/CH4 separation, J. Clean. Prod. 170 (2018) 704–714, https://doi.org/10.1016/j.jclepro.2017.09.169.
[30] M. Karimi, R.M. Siqueira, A.E. Rodrigues, F. Nouar, J.A.C. Silva, C. Serre, A. Ferreira, Biogas upgrading using shaped MOF MIL-160(Al) by pressure swing adsorption process: Experimental and dynamic modelling assessment, Sep. Purif. Technol. 344 (2024) 127260, https://doi.org/10.1016/j.seppur.2024.127260.
[31] H. Yan, Q. Fu, Y. Zhou, D. Li, D. Zhang, CO_2 capture from dry flue gas by pressure vacuum swing adsorption: A systematic simulation and optimization, Int. J. Greenh. Gas Control 51 (2016) 1–10, https://doi.org/10.1016/j.ijggc.2016.04.005.
[32] C.W. Skarstrom, Use of adsorption phenomena in automatic plant-type gas analyzers, Ann. n. y. Acad. Sci. 72 (1959) 751–763, https://doi.org/10.1111/j.1749-6632.1959.tb44201.x.
[33] A. Ali Abd, M. Roslee Othman, Z. Helwani, J. Kim, An overview of biogas upgrading via pressure swing adsorption: Navigating through bibliometric insights towards a conceptual framework and future research pathways, Energy Convers. Manag. 306 (2024) 118268, https://doi.org/10.1016/j.enconman.2024.118268.
[34] M. Azadi Tabar, H. Maghsoudi, K. Karimi, S.S. Hosseini, M. Gholami, J.F. M. Denayer, Techno-economic analysis of vacuum pressure swing adsorption process for a sustainable upgrading of biogas, J. Clean. Prod. 450 (2024) 141853, https://doi.org/10.1016/j.jclepro.2024.141853.
[35] W. Chen, W. Chen, R. Chein, K. Manatura, M. Ghorbani, Optimization of hydrogen purification from biomass-derived syngas via water gas shift reaction integrated with vacuum pressure swing adsorption for energy storage, Energy Storage 6 (2024) e604.
[36] Y. Chen, H. Ahn, Optimization strategy for enhancing the product recovery of a pressure swing adsorption through pressure equalization or co-current depressurization: A case study of recovering hydrogen from methane, Ind. Eng. Chem. Res. 62 (2023) 5286–5296, https://doi.org/10.1021/acs.iecr.2c04654.
[37] Y. Shen, W. Shi, D. Zhang, P. Na, B. Fu, The removal and capture of CO_2 from biogas by vacuum pressure swing process using silica gel, J. CO2 Util. 27 (2018) 259–271, https://doi.org/10.1016/j.jcou.2018.08.001.
[38] J. Xiao, L. Fang, P. Bénard, R. Chahine, Parametric study of pressure swing adsorption cycle for hydrogen purification using Cu-BTC, Int. J. Hydrog. Energy 43 (2018) 13962–13974, https://doi.org/10.1016/j.ijhydene.2018.05.054.
[39] G.N. Nikolaidis, E.S. Kikkinides, M.C. Georgiadis, Modelling and optimization of pressure swing adsorption (PSA) processes for post-combustion CO_2 capture from flue gas, in: A.I. Papadopoulos, P. Seferlis (Eds.), Process Syst. Mater. CO_2 Capture, 1st ed.,, Wiley, 2017, pp. 343–369, https://doi.org/10.1002/9781119106418.ch13.
[40] J.M. Lee, S. Lee, D.H. Kye, H.J. Park, W. Park, J. Shin, K. Park, Environ-economic analysis of high-temperature steam electrolysis for decentralized hydrogen production, Energy Convers. Manag. 266 (2022) 115856, https://doi.org/10.1016/j.enconman.2022.115856.
[41] J.M. Lee, S.H. Lee, J.H. Baik, K. Park, Techno-economic analysis of hydrogen production electrically coupled to a hybrid desalination process, Desalination 539 (2022) 115949, https://doi.org/10.1016/j.desal.2022.115949.
[42] S.H. Lee, J.D. Lee, D.-H. Lim, K. Park, Conceptual design of a sustainable hybrid desalination process using liquefied natural gas cold energy, ACS Sustain. Chem. Eng. 9 (2021) 13559–13572, https://doi.org/10.1021/acssuschemeng.1c04585.
[43] S.H. Lee, K. Park, Conceptual design and economic analysis of a novel cogeneration desalination process using LNG based on clathrate hydrate, Desalination 498 (2021) 114703, https://doi.org/10.1016/j.desal.2020.114703.
[44] G. Marcoberardino, D. Vitali, F. Spinelli, M. Binotti, G. Manzolini, Green hydrogen production from raw biogas: A techno-economic investigation of conventional processes using pressure swing adsorption unit, processes 6 (2018) 19. Doi: 10.3390/pr6030019.
[45] M. Draou, A. Brakez, A. Bennouna, Techno-economic feasibility assessment of a photovoltaic water heating storage system for self-consumption improvement purposes, J. Energy Storage 76 (2024) 109545, https://doi.org/10.1016/j.est.2023.109545.
[46] Ecoinvent 3.9.1, (2023). https://ecoinvent.org/database/ (accessed March 20, 2024).
[47] S. Lee, I. Lee, D. Seo, H. Kim, G. Joo, S. Lee, K. Park, Life cycle assessment of aPHA production, ACS Sustain. Chem. Eng. 12 (2024) 72–84, https://doi.org/10.1021/acssuschemeng.3c04788.
[48] ICAP Allowance Price Explorer, Int. Cabon Action Partnersh. ICAP (2024). https://icapcarbonaction.com/en (accessed July 10, 2024).
[49] Siemens 1996-2024, gPROMS process software (Siemens), Siemens (1996). https://www.siemens.com/global/en/products/automation/industry-software/gproms-digital-process-design-and-operations/gproms-modelling-environments/gproms-process.html (accessed March 21, 2024).
[50] D.D. Duong, Adsorption analysis: equilibria and kinetics, Imperial College Press, 1998.
[51] Z. Guan, Y. Wang, X. Yu, Y. Shen, D. He, Z. Tang, W. Li, D. Zhang, Simulation and analysis of dual-reflux pressure swing adsorption using silica gel for blue coal gas initial separation, Int. J. Hydrog. Energy 46 (2021) 683–696, https://doi.org/10.1016/j.ijhydene.2020.09.209.